Meccanica (2018) 53:305–317
https://doi.org/10.1007/s11012-017-0726-x

Developing a fast response SMA-actuated rotary actuator: modeling and experimental validation

Azadeh Doroudchi · Mohammad Reza Zakerzadeh · Mostafa Baghani

Received: 2 February 2017 / Accepted: 14 July 2017 / Published online: 25 July 2017

Abstract Shape memory alloy (SMA) applications as actuators are welcome nowadays due to their interesting properties. However, low speed and nonlinear behavior are two drawbacks of SMA. In order to overcome the latter disadvantages, this paper focuses on modeling, identification, and simulation of a fast response SMA-actuated rotary actuator. Genetic algorithm (GA) is used to identify unknown parameters of the model. In order to validate the model, a set-up is designed to provide experimental data. Using a pair of SMA wires in an antagonistic configuration helps improving the actuation speed and to reach bidirectional rotation without using springs. Furthermore, three modes of air convection cooling procedure are applied to the mechanism in order to provide faster responses. Finally, it is shown that the fast response rotary actuator is able to work within 5 Hz frequency bandwidth input electrical current providing 4° angle of rotation in high air convection cooling mode.

A. Doroudchi
Mechatronics Engineering Group, Alborz Campus, University of Tehran, Tehran, Iran
e-mail: doroudchi@ut.ac.ir

M. R. Zakerzadeh (✉) · M. Baghani
School of Mechanical Engineering, College of Engineering, University of Tehran, Tehran, Iran
e-mail: zakerzadeh@ut.ac.ir

M. Baghani
e-mail: baghani@ut.ac.ir

Keywords Shape memory alloy (SMA) · Rotary actuator · Modeling · Identification · Genetic algorithm (GA) · Experimental validation · Fast response

1 Introduction

In the last few years there has been a growing interest in the applications of shape memory alloy (SMA) materials including medical devices, orthodontic treatment, biotechnology, civil engineering structures, robotics, and mechanical systems. The most interesting properties of SMAs are large force-to-mass ratio, biocompatibility, light-weight, and noiseless operation when compared to the conventional DC motors [1]. In addition, compactness, silent and clean operation, and ability to develop extremely large recoverable strain are other useful properties of SMAs which make them suitable to be included in mechanical devices of small dimensions and to be used as actuating elements [2]. However, they have some disadvantages such as low speed and nonlinear behavior.

1.1 Some SMA applications

Numerous studies in SMA materials and their applications have been done in recent years. For instance, a push-pull actuator for commanding the motion of the interphalangeal joints of anthropomorphic robotic

hands was proposed in 1989 [3]. As another robotic application, an optimal design of an SMA actuator for microgrippers was done in 1997 [4]. In addition, two designs for an endoscopic tip, both actuated by SMAs were described in 1998 [5]. The authors' aim was to have 180° rotation available at the tip of the endoscope without any mechanical driving system connected to the surgeon. An overview of SMA behavior, modeling, and its' application in structural vibration control and seismic isolation was proposed in 2002 [6]. An SMA damper was used to mitigate the vibration of a stay cable in 2004, in which the control effectiveness could be influenced by the SMA damper parameters and locations [7]. A review of SMA materials applications for passive, active, and semi-active controls of civil structures was presented in 2006 [8]. Another application of SMA as damper was proposed in 2011 [9]. In the latter study, a hybrid solution combining wrapped SMA wires and an open-loop actuation was used to control multimodal cable vibrations. In 2012, opposing SMA elements were used in an antagonistic configuration to produce different motion paths and two-way mechanical work in a very efficient manner [10]. Recently, very comprehensive review papers on designing SMA linear actuators [11] and on SMA rotary actuators [12] were published. Most of the studies on SMA applications as actuators are mentioned in the latter papers. In addition, a very good classification of rotary actuators according to the types of rotation (continuous or non-continuous, single or reversible direction) was done in [12]. In the current study, a novel SMA-actuated rotary actuator has been designed and constructed in order to provide fast responses which can be useful in robotics applications.

1.2 SMA modeling

In order to predict the SMA nonlinear behavior, different models have been presented by Tanaka, Liang and Rogers, and Brinson. They have been analyzed and compared in [13]. These models have been used as SMA modeling methods in most of the previous studies. A robotic arm was used in order to enhance the phenomenological model to be able to predict the SMAs behavior under complex thermomechanical loading in 2005 [14]. An analytic model of a linear/rotary actuator was formed in 2011 [15], by using an SMA wire wounded over a cylindrical drum. A comparative analysis of some one-dimensional SMA constitutive models has been done based on experimental tests in 2012 [16]. As a result, it was shown that the Brinson model is more accurate than the others. The latter is discussed with more details in the modeling section of the present paper. In 2014, a phenomenological model was presented for microstructure-dependent inelasticity in SMAs [17]. In the same year, a dynamic multi-axial behavior of SMA nano-wires with coupled thermo-mechanical phase-field models was proposed [18]. Moreover, a paradigm for modeling SMA actuators through a rigorous experimental procedure was presented in [19]. It is indicated that by applying an efficient artificial system the behavior of SMA can be identified without any specific knowledge of the physical conditions and governing equations. In 2016, concept and modeling of using SMA was proposed in order to obtain variable compliance maps of a flexible structure [20]. Considering the literature work on SMAs' modeling, derivative form of Brinson model has been used in this study in order to predict the nonlinear behavior of the SMA wire.

1.3 SMA actuators with fast responses

As aforementioned, low speed is one of the SMA disadvantages. To this end, many studies have been done with the purpose of improving the response of SMA actuators. Early in 1995, an IR sensor was used in order to prevent the SMA overheating by measuring the wire temperature [21]. In the latter, the cooling procedure is improved by adding a mobile heat sink. In 2006, a light-weight heat sink consisting a metal tube with silicon grease was used to cool the wire effectively. A high current pulse was applied to fasten the SMA response and the highest measured frequency was 2 Hz [22]. In the same year, a method was used for improving the speed of actuators based on SMA through increasing the rate at which an SMA element can be safely heated [23]. The best reported result was 1 Hz frequency bandwidth without any change in SMA cooling regime. A unique experimental system has been developed in 2010 that applied a high-voltage electric pulse to a detwinned NiTi wire [24]. The characteristic rise time was identified as 50–100 μs based on one-occasional rapid Joule heating of SMA elements. Various active cooling techniques such as fluid flow and heat sink were investigated to improve

the response time of two commercially available SMAs [25]. Although the cooling period was decreased from 1.6 to 0.2 s, the maximum reached frequency bandwidth was 0.55 Hz. Later, a comparative theoretical study was conducted on the performance of a set of controllers to improve the speed of actuators based on SMA with 0.69 Hz bandwidth expected for continuous cyclic operation in 2012 [26]. The influence of temperature, stress, and strain on the speed operation of SMA were proposed in 2014 [27]. In the latter paper, the SMA wire frequency bandwidth was increased from 0.37 to 1 Hz. In 2016, the influence of cooling and heating rates on contraction of SMA were studied and identified [28]. The authors' aim was to find the maximum attainable frequency bandwidth which was reported as 0.15 Hz. To sum up, the literature does not contain any experimental results reporting the SMA operation frequency bandwidth higher than 2 Hz in the open-loop control mode.

The main contribution of this study is achieving 5 Hz frequency bandwidth for cyclic rotation of the designed rotary actuator. The antagonistic configuration and cooling method were the keys to reach fast responses. The behavior and response of SMA are influenced by heating and cooling methodologies, the wire diameter and length, and other experiment environment specifications. The efficient modeling and the convective heat transfer parameter identification helped predicting the behavior of the proposed SMA-actuated rotary actuator accurately. Therefore, the results of the present study are eligible to be compared to similar works despite all differences in the experimental implementations.

The reminder of the present paper is organized as follows. Section 2 describes the developed rotary actuator set-up. In Sect. 3, modeling, identification and simulation of the SMA actuator are discussed. Section 4 presents the experimental validation of the proposed model via obtained data from open-loop control of the system. The fastest responses of the proposed SMA-actuated rotary actuator are illustrated in Sect. 5. Finally, the paper concludes with some remarks and hints.

2 Set-up for the SMA-actuated rotary actuator

In the developed rotary actuator, the SMA wires are used in an antagonistic configuration in order to increase the actuator speed. This allows the rotary actuator to rotate in both directions without using springs. Therefore, a pulley is designed with two separated grooves around its environment surface in order to hold the SMA wires as it is shown in Fig. 1a. SMA wires used in this study are Flexinol actuator type[1] with 0.2 mm (0.08 inch) diameter and 50 cm length. The pulley radius (r) is 2 cm with 0.05 kg mass, and it is constructed with PTFE material which can tolerate the temperature up to 230 °C. The pulley is installed on a 3600 pulse rotary encoder[2] shaft. Thus, the rotary actuator angle (θ) could be calculated readily by counting the pulses that the encoder sends to the processor. Each SMA wire is connected to the pulley on one end while the other end is fixed to an S-type loadcell,[3] shown in Fig. 1b. The loadcells are used to provide force feedback for future planned closed-loop control methods. Figure 2 illustrates the designed set-up box for the rotary actuator with 60 cm length and 12 cm width. In addition, two micro-controllers[4] are used to send control commands to the two drivers[5] in order to provide the desired electrical currents for the SMA wires. The micro-processors read the output data of the electrical current sensors, encoder, and loadcells. Figure 3 shows the schematic of the whole system, in which, the relations between different parts of the SMA-actuated rotary actuator are clarified. As it is depicted, electrical currents are sent from control unit to the SMA wires which cause an increase in wires' temperature. Thus, the wires' recoverable strain makes the pulley rotate. Therefore, the system inputs are electrical currents and the system output is the pulley rotation angle. In this part of the study, the actuator control method is open-loop implying no feedback or reference input.

Another part of the design consists of high speed computer fans that help reducing the SMA wires cooling period. Two high speed fans are fixed at each end of the box in different directions in order to circulate the air along the box and three high speed fans are fixed in front of SMA wires. The latter fans could arbitrary be used during the experimental tests.

[1] Manufactured by Dynalloy Inc.

[2] Autonics - E50S Series.

[3] Lascaux - STC-5kg.

[4] Arduino Due and Arduino Mega.

[5] LMD5560-HV.

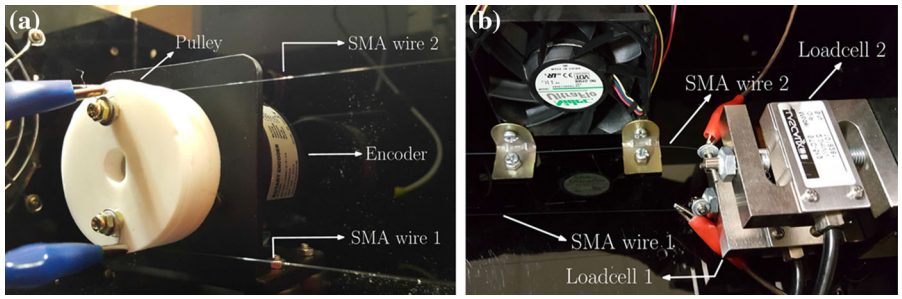

Fig. 1 SMA wires connections in rotary actuator. **a** Pulley connected to the encoder and SMA wires. **b** S-type loadcells connected to SMA wires

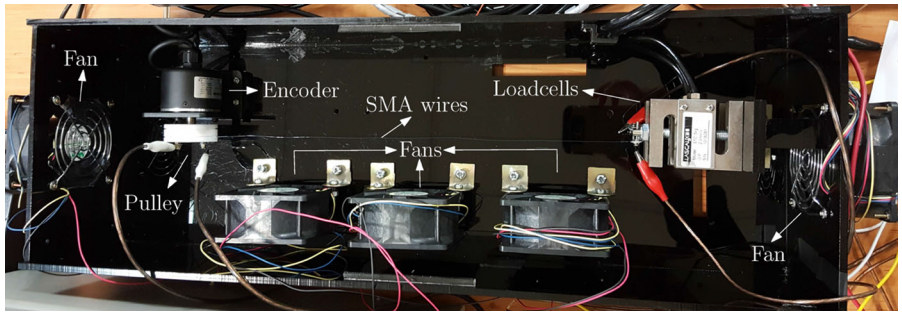

Fig. 2 Designed box for the rotary actuator

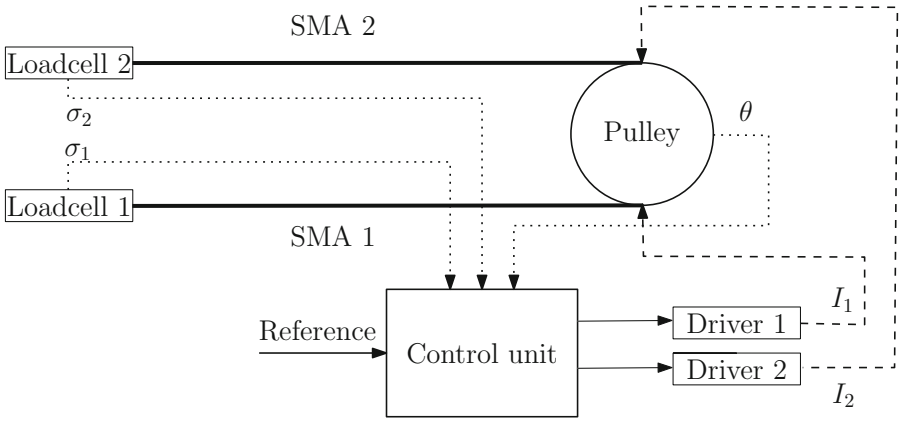

Fig. 3 Schematic of the SMA-actuated rotary actuator

Therefore, three main cooling procedures are defined as:

1. Free convection
2. Low air convection
3. High air convection

where, free convection is when the cooling fans are OFF. In low air convection, two fans are ON. In high air convection, all five fans are ON.

3 Modeling of the developed SMA-actuated rotary actuator

Modeling of SMA is challenging due to its nonlinear behavior. In addition, in order to model the whole SMA-actuated rotary actuator, the relation between the input and output of the system is needed to be found. Therefore, the SMA wire constitutive model, kinematics, and dynamics are discussed in the following subsections.

3.1 SMA wire constitutive model

Shape memory alloy wires could be used as actuators because of their change in physical characteristics during their phase transformations between high and low temperatures. There are two major phases: martensite and austenite. During the time that electrical current of SMA wire is increasing (heating process), the SMA wire phases change from martensite to austenite. During the time that the current is decreasing (cooling process), the austenite phase converts to martensite phase. The SMA wires behavior due to their phase changes are modeled by different scientists as discussed in [13, 16]. In the latter study done by Zakerzadeh et al., it is shown that the Brinson model with the corrected evolution kinetics developed by Chung et al. can model the behavior of SMA wires more accurately regarding the validation assessment of three major one dimensional constitutive SMA models with experimental data [13]. Figure 4 illustrates the critical stress-temperature profile used in Brinson model [13]. In Brinson model, the martensite phase is separated into two components named twinned martensite and detwinned martensite, which distinguishes it from other models. M_s, M_f, A_s, and A_f are four transformation temperatures which respectively mean martensite start, martensite finish, austenite start, and austenite finish temperatures. The detwinning start and finish stresses are shown as σ_s^{cr} and σ_f^{cr} in Fig. 4. The stress-influence coefficients, C_M and C_A, are the constants indicating the influence of stress on the transformation temperatures of martensite and austenite phases, respectively.

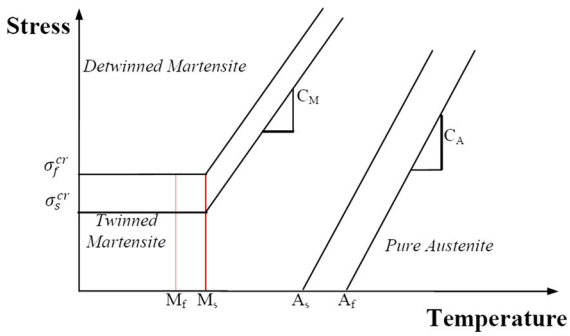

Fig. 4 The critical stress-temperature profile used in Brinson model [13]

In the current study, the following discussed model is used to provide the best and accurate model which can be considered as the closest one to the actual behavior of the system. In order to obtain reliable results from the model, it is necessary to use appropriate values for the constant parameters. The essential parameters are listed in Table 1 [13].

Table 1 SMA wire parameters

Parameter	Definition	Value	Unit
M_s	Martensite start temperature	48.4	°C
M_f	Martensite final temperature	43.9	°C
A_s	Austenite start temperature	68	°C
A_f	Austenite final temperature	73.8	°C
C_A	Austenite stress-influence coefficient	6.73	MPa °C^{-1}
C_M	Martensite stress-influence coefficient	6.32	MPa °C^{-1}
E_A	Austenite Young modulus	31.5	GPa
E_M	Martensite Young modulus	20	GPa
R_A	Austenite wire resistance	100	μΩ cm
R_M	Martensite wire resistance	80	μΩ cm
Θ_A	Austenite thermal expansion coefficient	11	μ Pa °C^{-1}
Θ_M	Martensite thermal expansion coefficient	6.6	μPa °C^{-1}
σ_s^{cr}	Detwinning start stress	25	MPa
σ_f^{cr}	Detwinning finish stress	78	MPa
ε_L	Maximum recoverable strain	4.1	%
D	SMA wire diameter	0.2	mm
C_p	Thermal capacity of SMA wire	2.046	MJ m^{-3} °C

In order to use the Brinson constitutive model in dynamic equations of the proposed rotary actuator, it is more effective to use the differential form of the mentioned constitutive model as follows [29]:

$$\dot{\sigma} = E(\xi)(\dot{\varepsilon} - \varepsilon_L \dot{\xi}_s) + \dot{\xi}(E_M - E_A)(\varepsilon - \varepsilon_L \xi_s) + \Theta \dot{T} \tag{1}$$

where σ, ε and ε_L are the SMA wire stress, strain, and the maximum recoverable strain, respectively. T is the temperature and Θ is related to the thermal coefficient of expansion of the SMA wire [30]. E is the SMA module of elasticity which is usually assumed to be a linear function of the martensite volume fraction:

$$E(\xi) = E_A + \xi(E_M - E_A) \tag{2}$$

in turn, the SMA martensite volume fraction (ξ) is separated into stress-induced fraction (ξ_s) and temperature-induced fraction (ξ_T) as follows:

$$\xi = \xi_s + \xi_T \tag{3}$$

In the Brinson model, the phase domains are separated by some boundaries as are illustrated in Fig. 4. Therefore, for each of the phase conversions, the evolution equations which calculate the martensite fraction as a function of stress and temperature are represented [29]:

- Conversion to detwinned martensite:

$$\begin{aligned}
&\text{For } \mathrm{T} > \mathrm{M_s} \ \&\ \sigma_{\mathrm{s}}^{\mathrm{cr}} + \mathrm{C_M}(\mathrm{T} - \mathrm{M_s}) \\
&< \sigma < \sigma_f^{cr} + C_M(T - M_s) \\
&\dot{\xi}_s = -\frac{1-\xi_{s0}}{2} \sin\left(\frac{\pi}{\sigma_{\mathrm{s}}^{\mathrm{cr}} - \sigma_{\mathrm{f}}^{\mathrm{cr}}}\left[\sigma - \sigma_{\mathrm{f}}^{\mathrm{cr}} - \mathrm{C_M}(\mathrm{T} - \mathrm{M_s})\right]\right) \\
&\frac{\pi}{\sigma_s^{cr} - \sigma_f^{cr}}(\dot{\sigma} - C_M \dot{T}) \\
&\dot{\xi}_T = -\frac{\xi_{T0}}{1-\xi_{s0}} \dot{\xi}_s
\end{aligned} \tag{4}$$

$$\begin{aligned}
&\text{For} \quad T < M_s \quad \& \quad \sigma_s^{cr} < \sigma < \sigma_f^{cr} \\
&\dot{\xi}_s = -\frac{1-\xi_{s0}}{2} \sin\left(\frac{\pi(\sigma - \sigma_f^{cr})}{\sigma_s^{cr} - \sigma_f^{cr}}\right) \frac{\pi}{\sigma_s^{cr} - \sigma_f^{cr}} \dot{\sigma} \\
&\dot{\xi}_T = -\frac{\dot{\xi}_s}{1-\xi_{s0}} \Delta_{T\varepsilon} + \frac{1-\xi_s}{1-\xi_{s0}} \dot{\Delta}_{T\varepsilon} \\
&\text{where,} \\
&\text{if} \quad M_f < T < M_s \quad \& \quad T < T_0 \\
&\dot{\Delta}_{T\varepsilon} = -\frac{1-\xi_{s0}-\xi_{T0}}{2} \sin\left(a_M[T - M_f]\right) a_M \dot{T} \\
&\text{else} \\
&\dot{\Delta}_{T\varepsilon} = 0
\end{aligned} \tag{5}$$

- Conversion to austenite:

$$\begin{aligned}
&\text{For} \quad T > A_s \quad \& \quad C_A(T - A_f) < \sigma < C_A(T - A_s) \\
&\dot{\xi} = -\frac{\xi_0}{2} \sin\left(a_A\left[T - A_s - \frac{\sigma}{C_A}\right]\right)\left(a_A\left[\dot{T} - \frac{\dot{\sigma}}{C_A}\right]\right) \\
&\dot{\xi}_s = \frac{\xi_{s0}}{\xi_0} \dot{\xi} \\
&\dot{\xi}_T = \frac{\xi_{T0}}{\xi_0} \dot{\xi}
\end{aligned} \tag{6}$$

In the above equations, $a_M = \pi/(M_s - M_f)$ and $a_A = \pi/(A_f - A_s)$ are two material constants in terms of transition temperatures. Moreover, the parameters with zero index are the initial values of the related parameter.

The heat transfer equation for one dimensional horizontal SMA wire assuming uniformed temperature in wire area is simplified as [31]:

$$C_p \frac{\mathrm{d}T(t)}{\mathrm{d}t} = -\frac{4}{D} h(T)[T(t) - T_0] + RJ^2 \tag{7}$$

where, T is the SMA wire temperature and t is time. C_p, D, and h are the thermal capacity, SMA wire diameter, and the convective heat transfer coefficient, respectively. R is the electrical resistivity of the SMA wire and J is the electrical current density. Since the SMA wire resistivity changes during phase transformation, it is continuously updated using the following equation:

$$R(\xi) = R_A + \xi(R_M - R_A) \tag{8}$$

The heat transfer equation plays a crucial role in the phase transformations of the SMA wire due to the temperature changes. The most sensitive parameter, which has a very large impact on the stability of the model, is the SMA wire convective heat transfer coefficient (h).

The proposed SMA wire heat transfer equation specifies the relation between the SMA wire electrical current and temperature. In addition, SMA wire stress and strain are calculated in the constitutive model. Therefore, the present modeling will be completed by taking advantage of the kinematic and dynamic models.

3.2 Kinematic and dynamic models

The SMA wire strain (ε) changes from 0 to 4% during electrical excitation. The latter causes the change of

SMA wire length (l) during actuation. In the proposed mechanism, the change in SMA wire length is used to rotate a pulley in both directions. In addition, due to antagonistic configuration, each SMA wire strain changes 2% during actuation. The kinematic equation of the rotary actuator explains the relationship between the angle of rotation and the SMA wire strain as:

$$r\theta = \varepsilon l \tag{9}$$

in which, ε could be replaced by ε_1 and ε_2 for SMA wire one and SMA wire two, respectively (Attn: $\varepsilon_1 = -\varepsilon_2$). In addition, each SMA wire applies force to the pulley when it is actuated. The dynamic equation relating the SMA wires forces (F_{SMA1} and F_{SMA2}) and

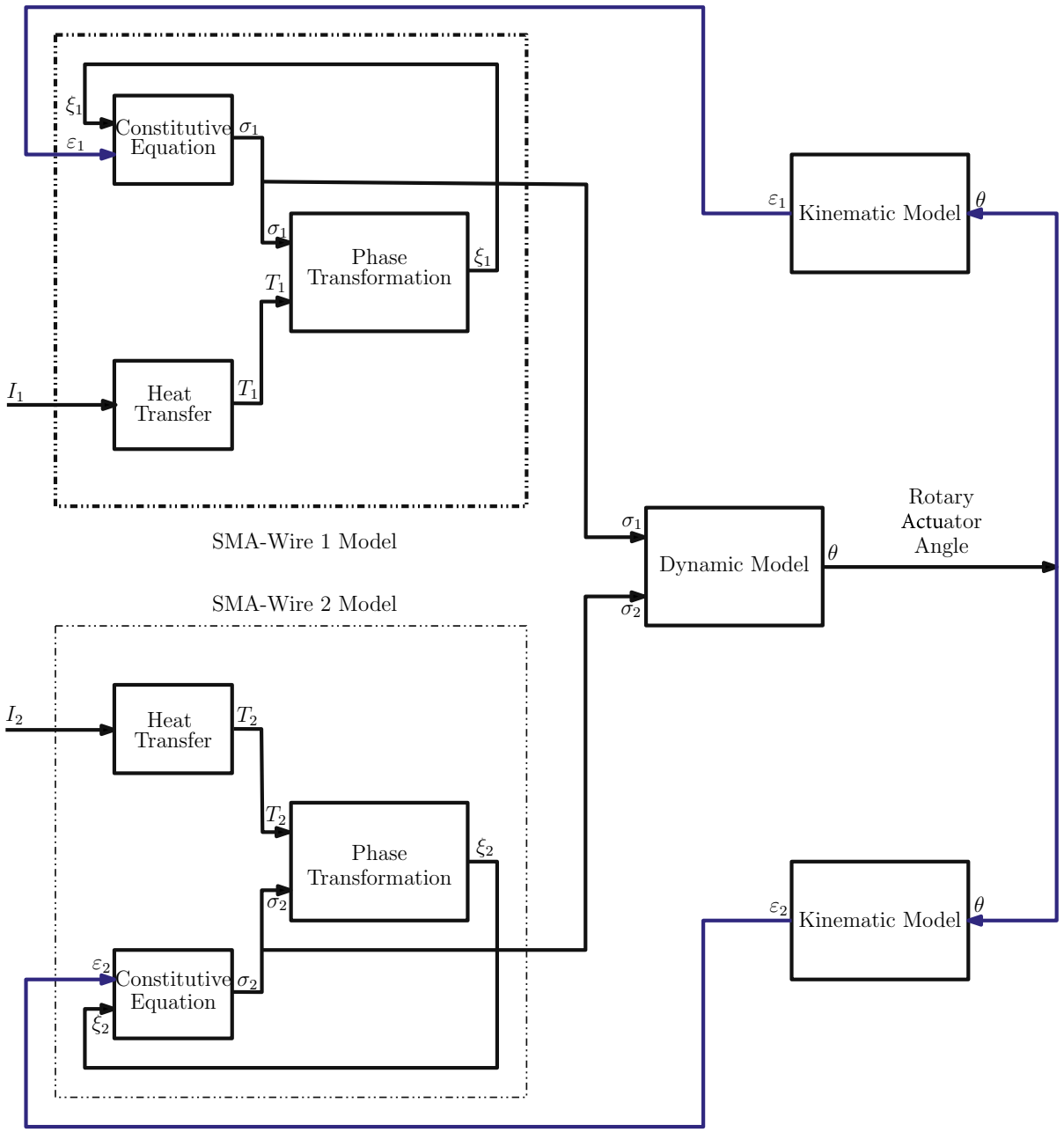

Fig. 5 Block diagram of the SMA-actuated rotary actuator modeling

the rotary actuator angular acceleration ($\ddot{\theta}$) is presented in the following equation:

$$(F_{SMA1} - F_{SMA2}) \times r = I_e \ddot{\theta} \quad (10)$$

where, I_e is the effective mass moment of inertia of the pulley. Force equation for each wire is $F = \sigma A$, in which, A is the cross-section area of SMA wire ($A = \pi D^2/4$). Moreover, $\ddot{\theta}$ is the angular acceleration. The rotation angle of the actuator is then calculated by twice integrating the acceleration during each iteration of the simulation.

3.3 Convective heat transfer coefficient identification

The convective heat transfer coefficient (h) depends on SMA wire environmental conditions. Therefore, it is identified in different cooling procedures using input-output data of the rotary actuator. However, previous studies used the temperature sensor data (which suffers from delay and noise) to calculate h from heat transfer equations [25, 28]. The convective heat transfer coefficient could be estimated as a polynomial with respect to the SMA temperature (T). According to the literature [14, 25, 28] and in order to obtain less complex estimation, it is identified in term of a second order polynomial as:

$$h(T) = h_0 + h_1 T + h_2 T^2 \quad (11)$$

where, h_0, h_1, and h_2 are assumed to be constant. It is found that h_0 could be selected from 70 to 1000 and h_1, h_2 between 0 and 1. As h_2 has more influence on the final h value with respect to h_1 and in order to prevent complexity, two different forms of the presented polynomials are considered. First order polynomial ($h_2 = 0$) and second order polynomial (while $h_1 = 0$). Therefore, there are two coefficients to be identified in each of the proposed polynomials.

The proposed model of the rotary actuator is simulated in MATLAB simulink software. The block diagram of the model simulation is illustrated in Fig. 5. Similar to the physical actuator, the simulation inputs and output are the SMA wires electrical currents and the actuator rotation angle, respectively. Since there are two SMA wires in the proposed actuator, two similar but separated blocks are designed to simulate the SMA wires model. Each SMA wire block contains three internal blocks namely phase transformation, heat transfer, and constitutive equation. Moreover, the kinematic and dynamic models are simulated in individual blocks.

Genetic algorithm (GA) method is used in order to identify the unknown coefficients of h. The current GA method provides random values for each of the unknown parameters. An initial guess between 0 and 1 is made and mapped to the final values. In each iteration, the proposed simulation is run using the random values for the unknown parameters and the output is compared to the experimental data. The cost

Table 2 The specification of the genetic algorithm

Parameter	Value	Parameter	Value
Population	10	Iteration	100
Mutation percentage	30	Crossover Percentage	80
Mutation rate	0.02	Crossover adjustment	0.05

Table 3 Modeling errors respect to experimental train and test data

Polynomial model	Train data		Test data	
	Current (A)	RMSE (°)	Current (A)	RMSE (°)
Free convection				
First order	0.6	4.42	0.5	4.63
Second order	0.6	1.99	0.5	2.15
Low air convection				
First order	0.8	3.49	1.0	4.25
Second order	0.8	1.25	1.0	2.39
High air convection				
First order	1.0	4.57	1.2	7.06
Second order	1.0	3.16	1.2	3.93

function is the Root Mean Square Error (RMSE). At the end of each iteration, the values with the minimum cost function are selected as the best solution. The simulation running with random values could make the system unstable in some iterations. Therefore, the problem is solved by specifying a limit for the temperature value in the program. The population, mutation, and crossover parameter values are represented in Table 2. In addition, the crossover procedure is performed based on the so-called Roulette Wheel Selection.

In order to gather experimental data for the identification process, different values of electrical currents are applied to SMA wires in each of the three mentioned cooling procedures. The acquired data is

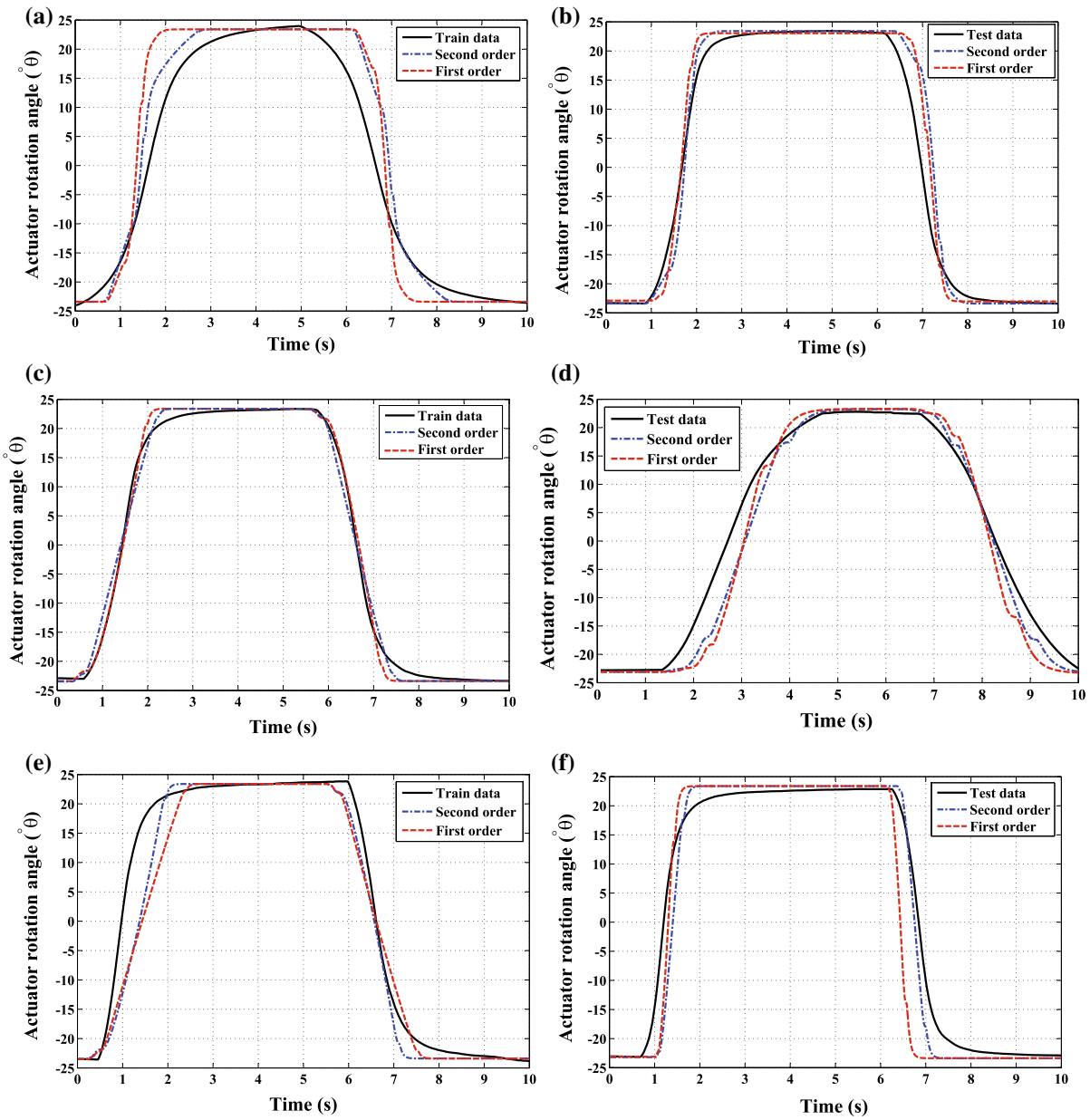

Fig. 6 Actuator rotation angle versus time in the training and test processes compared with the prediction of the model simulation for different cooling procedures as well as convective heat transfer coefficient identified for the first and second order polynomials of h. **a** Free convection training data. **b** Free convection test data. **c** Low air convection training data. **d** Low air convection test data. **e** High air convection training data. **f** High air convection test data

Table 4 Optimum values of convective heat transfer coefficients

Cooling method	h_0	h_1
First order polynomial		
Free convection	73.994	0.105
Low air convection	380.893	0.625
High air convection	660.135	0.423
Second order polynomial		
Free convection	100.614	0.001
Low air convection	160.381	0.041
High air convection	377.375	0.050

split into a training and testing set for use by the GA program. Table 3 illustrates the RMSE values of the experimental training and test data with respect to the simulation output. Low amount of RMSE values validates the accuracy of the identification. It should be mentioned that the frequency of the applied electrical currents is 0.1 Hz. The latter provides enough time for the SMA wires to reach their maximum recoverable strain. Figure 6 illustrates the selected cycles of the actuator rotation angle for each state of Table 3. Optimum values of the convective heat transfer coefficient are listed in Table 4. Since the RMSE values of the second order polynomial are less than the

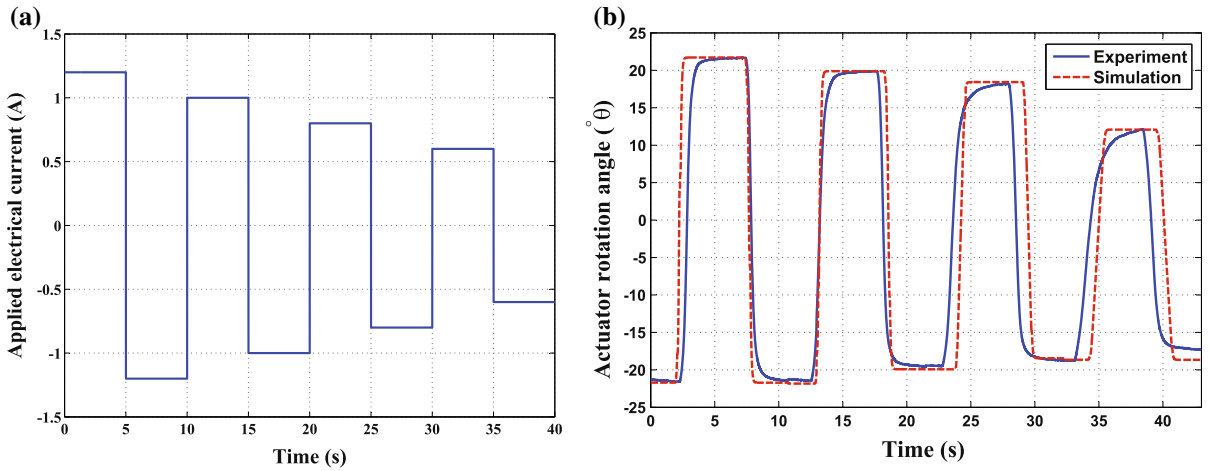

Fig. 7 Experimental actuator rotation angle in comparison to the model simulation while decaying square current is applied to the SMA wires. **a** Decaying square input applied as electrical current to SMA wires. **b** Actuator rotation angle with RMSE = 8.7°

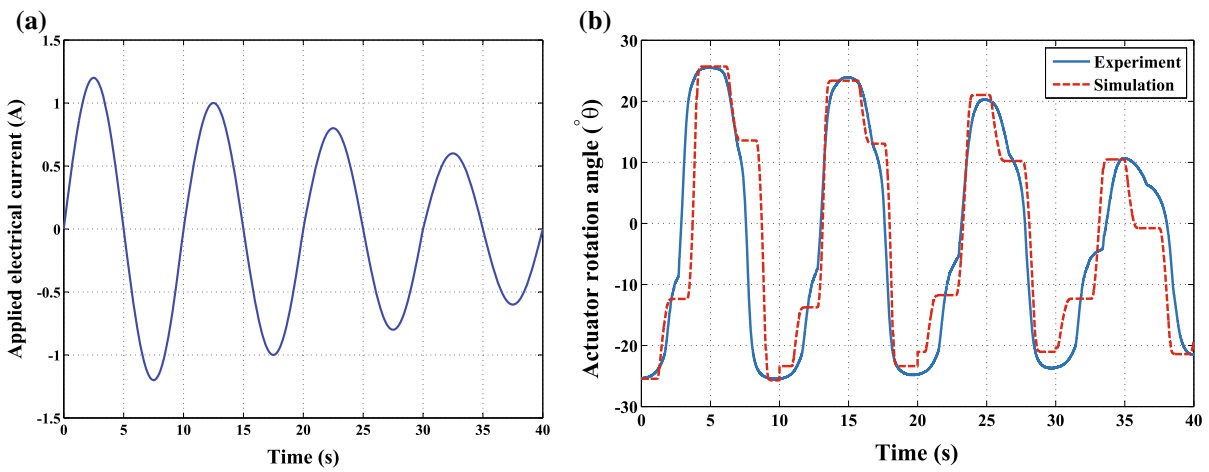

Fig. 8 Experimental actuator rotation angle in comparison to the model simulation while decaying sinusoidal current is applied to the SMA wires. **a** Decaying sinusoidal input applied as electrical current to SMA wires. **b** Actuator rotation angle with RMSE = 8.45°

first order polynomial, they are selected to finalize the simulation model.

4 Experimental validation of the proposed model

In this section, more complicated inputs are applied to the system in order to validate the finalized model. In addition, the system outputs repeatability is studied during the experimental tests. Therefore, the reported results are valid over time.

One of the latter inputs is square pulse with decreasing amplitude and the other one is a sinusoidal signal with decaying amplitude. The latter inputs cause minor hysteresis loops but the output results illustrate that the model is still valid for the minor hysteresis loops. In addition, the input current frequency is 0.1 Hz which is applied to SMA wires in free convection cooling method via open-loop control. Figure 7a illustrates the square pulse applied to the SMA wires in which, the positive part of the pulse is applied to SMA wire 1 and the negative part is applied to SMA wire 2. The system output is depicted in Fig. 7b. The decaying sinusoidal input and output are depicted in Fig. 8. Although the RMSE amounts are not negligible, it could be concluded that the proposed model is close to the behavior of the actual system. Since there is no feedback in the current control system, it is natural that the open-loop control is not strong or robust enough to follow the desired input so

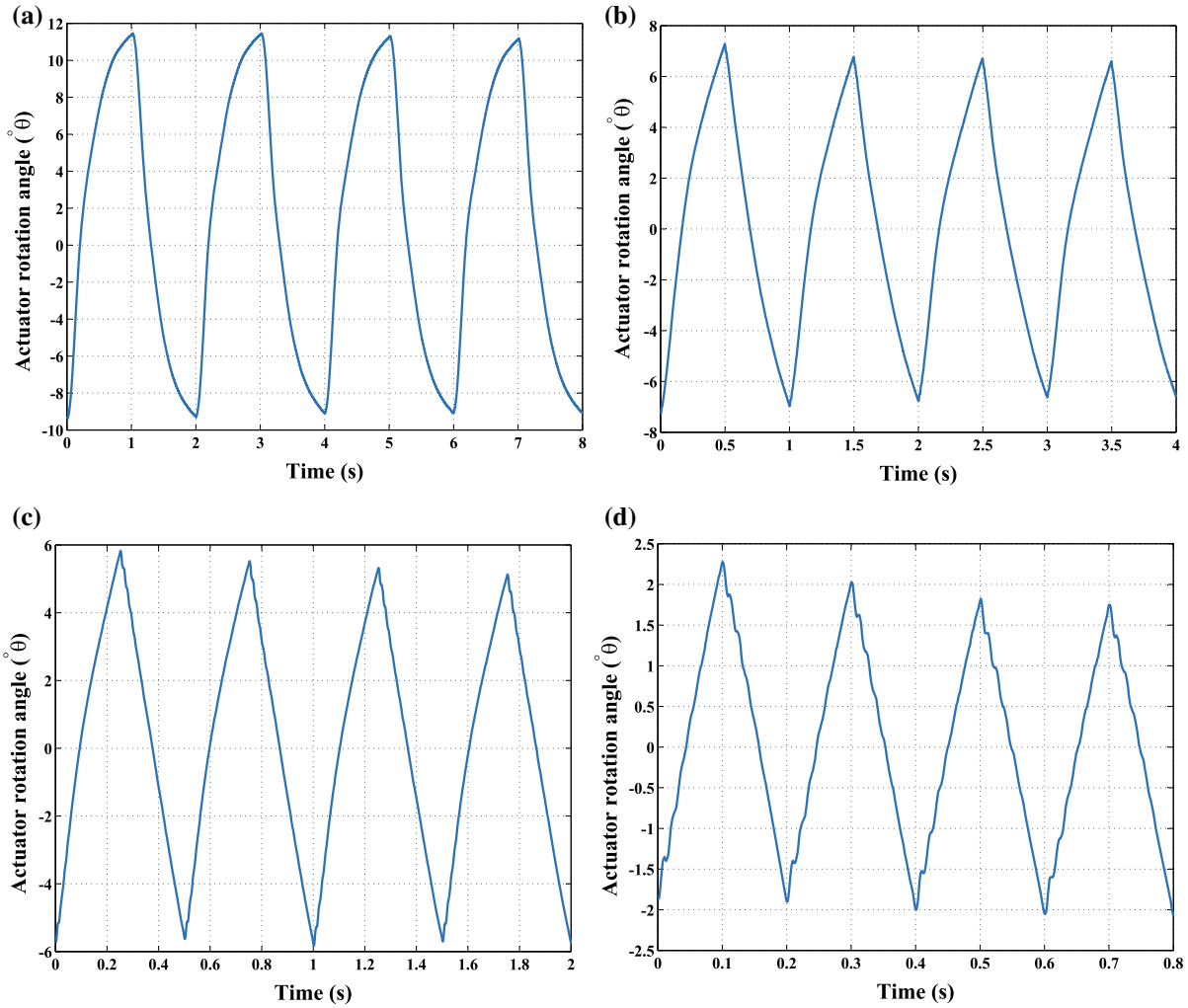

Fig. 9 SMA rotary actuator output angle in the fast response experimental tests via open-loop control. **a** 0.5 Hz frequency. **b** 1 Hz frequency. **c** 2 Hz frequency. **d** 5 Hz frequency

accurately. Therefore, a closed-loop control method could provide more accurate results in tracking a desired reference.

5 Fast response experimental results

As aforementioned, one goal of this study is to obtain high frequency responses from SMA actuator. Since the high air convection cooling method provides better heat convection, bigger amount of electrical currents could be applied to SMA wires. As a result, higher frequency outputs could be obtained. The maximum applicable electrical currents are predicted from the model and considered during the tests. The applied electrical currents to SMA wire 1 and 2 are complementary. The latter means that when one wire is actuated, the other wire is in rest and vice versa. The rotation angle of the SMA actuator after applying high frequency inputs are illustrated in Fig. 9. As depicted in Fig. 9d, 5 Hz is the highest obtained frequency with 4° peak-to-peak angle of rotation. It should be mentioned that the proposed SMA rotary actuator could even work at 10 Hz frequency providing 1° peak-to-peak angle of rotation. Therefore, the 5 Hz frequency result is reported as the best reasonable achievement of this study. Moreover, higher input currents with the same amount of frequencies are applied to SMA wires, but the maximum reachable angle of rotation cannot increase due to limitation of heat convection rate. However, by using longer SMA wires or by decreasing the pulley radius, the maximum reachable angle of rotation could easily be increased.

6 Conclusion

In this study, a fast response SMA-actuated rotary actuator was designed and constructed. An accurate modeling and identification were done using experimental data. Cooling fans and antagonistic configuration of SMA wires were two components which helped accelerating SMA wires performance. Finally, 5Hz frequency response of the proposed rotary actuator could be considered as a big step in improving SMA actuators' speed comparing to the achievements of previous studies. The abilities of SMA actuators in applying large amount of force and working in higher frequencies (which is shown in the present study) make them more efficient to be used in robotic applications. As future work, closed-loop control methods on the presented SMA actuator are in progress via position and force feedback.

Acknowledgements The authors would like to thank Mohammad Sharifzadeh and Amir Salimi for their cooperation.

References

1. Tabrizi VA, Moallem M (2007) July. Nonlinear position control of antagonistic shape memory alloy actuators. In: American control conference, 2007 (ACC'07). IEEE, pp 88–93
2. Nespoli A, Besseghini S, Pittaccio S, Villa E, Viscuso S (2010) The high potential of shape memory alloys in developing miniature mechanical devices: a review on shape memory alloy mini-actuators. Sens Actuators A 158(1):149–160
3. Bergamasco M, Salsedo F, Dario P (1989) A linear SMA motor as direct-drive robotic actuator. In: Proceedings of the 1989 IEEE international conference on robotics and automation. IEEE, pp 618-623
4. Troisfontaine N, Bidaud P (1997) Optimal design of a shape memory alloy actuator for microgrippers. In: ROMANSY 11. Springer, Vienna, pp 123–130
5. Peirs J, Reynaerts D, Van Brussel H (1998) Design of a shape memory actuated endoscopic tip. Sens Actuators A 70(1–2):135–140
6. Saadat S, Salichs J, Noori M, Hou Z, Davoodi H, Bar-On I, Suzuki Y, Masuda A (2002) An overview of vibration and seismic applications of NiTi shape memory alloy. Smart Mater Struct 11(2):218
7. Li H, Liu M, Ou J (2004) Vibration mitigation of a stay cable with one shape memory alloy damper. Struct Control Health Monit 11(1):21–36
8. Song G, Ma N, Li HN (2006) Applications of shape memory alloys in civil structures. Eng Struct 28(9):1266–1274
9. Faravelli L, Fuggini C, Ubertini F (2011) Experimental study on hybrid control of multimodal cable vibrations. Meccanica 46(5):1073–1084
10. Georges T, Brailovski V, Terriault P (2012) Characterization and design of antagonistic shape memory alloy actuators. Smart Mater Struct 21(3):035010
11. Mohd Jani J, Leary M, Subic A (2017) Designing shape memory alloy linear actuators: a review. J Intell Mater Syst Struct 28(13):1699–1718
12. Yuan H, Fauroux JC, Chapelle F, Balandraud X (2017) A review of rotary actuators based on shape memory alloys. J Intell Mater Syst Struct 28(14):1863–1885
13. Zakerzadeh MR, Salehi H (2009) Comparative analysis of some one-dimensional SMA constitutive models for a Ni–Ti wire for shape control applications with experimental data. In: Proceeding of 20th international conference on adaptive structures and technologies, Hong Kong, vol 8
14. Elahinia MH, Ahmadian M (2005) An enhanced SMA phenomenological model: II. The experimental study. Smart Mater Struct 14(6):1309

15. Scir Mammano G, Dragoni E (2011) Modeling of wire-on-drum shape memory actuators for linear and rotary motion. J Intell Mater Syst Struct 22(11):1129–1140
16. Sayyaadi H, Zakerzadeh MR, Salehi H (2012) A comparative analysis of some one-dimensional shape memory alloy constitutive models based on experimental tests. Sci Iran 19(2):249–257
17. Grandi D, Stefanelli U (2014) A phenomenological model for microstructure-dependent inelasticity in shape-memory alloys. Meccanica 49(9):2265–2283
18. Dhote RP, Melnik RNV, Zu J (2014) Dynamic multi-axial behavior of shape memory alloy nanowires with coupled thermo-mechanical phase-field models. Meccanica 49(7):1561–1575
19. Mozaffari A, Fathi A, Azad NL (2014) Preferred design of recurrent neural network architecture using a multiobjective evolutionary algorithm with un-supervised information recruitment: a paradigm for modeling shape memory alloy actuators. Meccanica 49(6):1297–1326
20. Mekaouche A, Chapelle F, Balandraud X (2016) Using shape memory alloys to obtain variable compliance maps of a flexible structure: concept and modeling. Meccanica 51(6):1287–1299
21. Russell RA, Gorbet RB (1993) Improving the response of SMA actuators. In: IEEE international conference on robotics and control, vol 1, no 3, pp 2299–2299
22. Loh CS, Yokoi H, Arai T (2006) Natural heat-sinking control method for high-speed actuation of the SMA. Int J Adv Rob Syst 3(4):42
23. Featherstone R, Teh Y (2006) Improving the speed of shape memory alloy actuators by faster electrical heating. Experimental robotics IX, pp 67–76
24. Vollach S, Shilo D (2010) The mechanical response of shape memory alloys under a rapid heating pulse. Exp Mech 50(6):803–811
25. Tadesse Y, Thayer N, Priya S (2010) Tailoring the response time of shape memory alloy wires through active cooling and pre-stress. J Intell Mater Syst Struct 21(1):19–40
26. Velzquez R, Pissaloux EE (2012) Modelling and temperature control of shape memory alloys with fast electrical heating. Int J Mech Control 13:1–8
27. Nakshatharan SS, Ruth DJS, Dhanalakshmi K (2015) Dynamic stabilization and rapid motion control system driven by antagonistic shape memory alloy actuators. J Vib Control 21(16):3189–3204
28. Lara-Quintanilla A, Bersee HE (2016) A study on the contraction and cooling times of actively cooled shape memory alloy wires. J Intell Mater Syst Struct 27(3):403–417
29. Basaeri H, Yousefi-Koma A, Zakerzadeh MR, Mohtasebi SS (2014) Experimental study of a bio-inspired robotic morphing wing mechanism actuated by shape memory alloy wires. Mechatronics 24(8):1231–1241
30. Brinson LC (1993) One-dimensional constitutive behavior of shape memory alloys: thermomechanical derivation with non-constant material functions and redefined martensite internal variable. J Intell Mater Syst Struct 4(2):229–242
31. Zakerzadeh MR, Salehi H, Sayyaadi H (2011) Modeling of a nonlinear Euler–Bernoulli flexible beam actuated by two active shape memory alloy actuators. J Intell Mater Syst Struct 22(11):1249–1268